Mechanism and Machine Theory 44 (2009) 835–849

Contents lists available at ScienceDirect

Mechanism and Machine Theory

journal homepage: www.elsevier.com/locate/mechmt

Dynamics and control of a planar 3-DOF parallel manipulator with actuation redundancy

Jun Wu *, Jinsong Wang, Liping Wang, Tiemin Li

Institute of Manufacturing Engineering, Department of Precision Instruments, Tsinghua University, Beijing 100084, PR China

ARTICLE INFO

Article history:
Received 6 December 2006
Received in revised form 14 March 2008
Accepted 9 April 2008
Available online 19 May 2008

Keywords:
Dynamics
Position and force switching control
Parallel manipulator
Actuation redundancy

ABSTRACT

This paper deals with the dynamics and control of a planar 3-DOF parallel manipulator with actuation redundancy. According to the kinematics of the redundant manipulator, the inverse dynamics is derived by using the virtual work principle, and the driving force is optimized by utilizing the least-square method. Based on the dynamic model, a position and force switching control strategy is proposed for the parallel manipulator. In this control strategy, two extendible links are controlled by position and force modes, respectively. Moreover, in the whole workspace, their control modes are switched. The critical angles for switching control modes are planned and the position compensation method is investigated. The control tests show that the contour error of the redundantly actuated parallel manipulator is similar to that of its corresponding non-redundant parallel manipulator without one extendible link. However, the redundant parallel manipulator has a larger orientation workspace and higher stiffness. The redundantly actuated parallel manipulator is incorporated into a 4-DOF hybrid machine tool which also includes a feed worktable.

1. Introduction

In theory, parallel manipulators are capable of answering the increasing needs of industry in terms of automation. The nature of their architectures tends to reduce absolute positioning and orienting errors. However, these manipulators have smaller workspace. In addition, works on singularities of parallel manipulators [1–4] show that static singularities (which are completely absent in open-chain serial manipulators) appear within the workspace with continuous region thereby rendering the manipulator uncontrollable in some regions of the workspace. It has been shown that actuation redundancy can be an effective solution for eliminating singularities in parallel manipulator designs and thus improving their performances [5].

So far as redundancy is concerned, redundancy can be classified into different types. Kinematic redundancy and actuation redundancy are more used. A manipulator is called kinematically redundant if it possesses more DOF than that is necessary for performing a specified task. Alternatively, a manipulator with actuation redundancy has more joint actuators than that are required to provide the desired end-effector motion. For a parallel manipulator, actuation redundancy can be obtained by replacing passive joints of the existing parallel manipulator with active ones or by introducing additional limbs in the existing system. It is noted that actuation redundancy does not affect the mobility of a parallel manipulator and only increases the number of actuators [6]. Actuation redundancy can be used to eliminate force-unconstrained configurations [7–9] or to satisfy actuator constrains [10,11]. At the same time, it enables the system to modulate the end-effector stiffness by realizing an internal load distribution [12]. Some applications of redundant actuation are found in systems such as multifingered robotic hands [13], haptic displays [14], and parallel machining centers [15].

* Corresponding author. Tel.: +86 10 62772633; fax: +86 10 62782351.
E-mail address: wu-j03@mails.tsinghua.edu.cn (J. Wu).

0094-114X/$ - see front matter © 2008 Elsevier Ltd. All rights reserved.
doi:10.1016/j.mechmachtheory.2008.04.002

As more actuators are added, the generating internal forces is possibly introduced, which leads to challenging control issues. It means that the use of mere position control is no longer possible. In order to apply the vast control literature developed for the serial counterparts to redundantly actuated parallel manipulators, it is necessary to develop an efficient dynamic model. There are many papers on dynamics and control of parallel manipulators with non-redundant actuation [16–19]. However, research on dynamics and control of redundantly actuated parallel manipulators is relatively fewer. Liu et al. [20] looked at both kinematic and dynamic control algorithms for redundantly actuated parallel manipulators. Cheng et al. [21] used computed control method to control a redundantly actuated parallel manipulator and tested the algorithms on a 2-DOF device. Ganovski et al. [22] introduced a feed-forward controller to control the redundantly actuated parallel mechanisms. Ropponen [23] used computed torque control and feed-forward control to control a redundantly actuated parallel manipulator, respectively. Further, the two methods were compared and the conclusion that computed torque control can obtain a better effect was drawn.

Moreover, some other methods are also discussed. Chakarov [24] developed a stiffness control scheme for parallel manipulators with actuation redundancy. Muller [25] developed an open-loop preload control and applied it to the elimination of backlash for redundantly actuated parallel manipulators. Kock and Schumacher [26] adopted decoupled control for a 2-DOF parallel manipulator with actuation redundancy. Shen et al. [27] introduced adaptive control for a redundantly actuated parallel manipulator. Kvtoslav et al. [28] discussed state-space generalized predictive control for redundant parallel manipulators. However, these control methods were tested only by simple tests or computer simulation since only a few prototypes of redundantly actuated parallel manipulators are developed. Further, the experimental results of some control methods were not ideal. To control an industrialized parallel manipulator, these control methods should be validated by more experiments.

In this paper, utilizing the virtual work principle, the dynamic model of a redundantly actuated parallel manipulator is derived. Based on the dynamic formulation, a position and force switching control method is proposed for the two extendible links. At one time, one of the two extendible links is controlled by the position mode and the other the force mode. In the whole workspace, the control modes of the two extendible links are switched. A few orientation angles are selected as the possible critical angles for switching control modes. By combining the parallel manipulator with a feed worktable, a 4-DOF hybrid machine tool is created to perform 4-axis tasks.

2. Structure description and kinematic analysis

2.1. Structure description

The redundantly actuated parallel manipulator is composed of a gantry frame, a moving platform, two constant length links and two extendible links, as shown in Fig. 1. The kinematic model of the parallel manipulator is shown in Fig. 2. Sliders E_1D_1 and E_2D_2 are actuated by two actuators and drive links A_1D_1 and A_2D_2. Links E_1B_1 and E_2B_2, which are driven by two actuators, are extendible struts with one end joined with sliders E_1D_1 and E_2D_2 and the other connected to the moving platform A_2B_2. P_1 and P_2 are counterweights, and link E_1B_1 is actuated by an active actuator which is redundant.

The universally accepted theory of DOF is that of Kutzbach Grübler. The Kutzbach Grübler formula with planar mechanism can be written as

$$M = 3(n - j - 1) + \sum_{i=1}^{j} f_i \tag{1}$$

where n is the number of the total members of the system, j is the number of the total kinematic pairs, and f_i is the DOF number of the ith kinematic pair.

Here, $n = 10$, $j = 12$, $\sum_{i=1}^{j} f_i = 12$. Thus, $M = 3(10 - 12 - 1) + 12 = 3$. Namely, the DOF number of the parallel manipulator is 3. The parallel manipulator is redundantly actuated since it has four actuators and only a 3-DOF output.

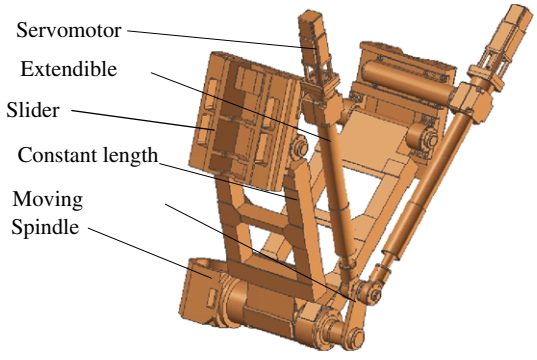

Fig. 1. 3-D model of the redundant parallel manipulator.

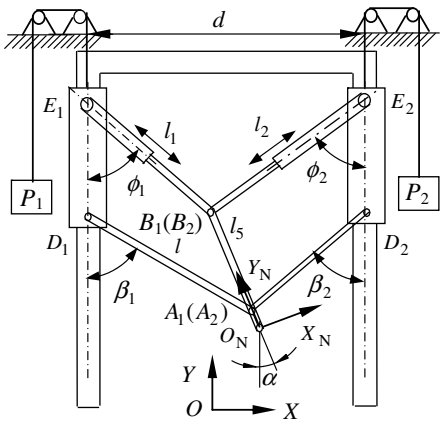

Fig. 2. Kinematic model of the redundantly actuated parallel manipulator.

2.2. Inverse kinematics

In practical application, the redundant parallel manipulator can be a subpart of a hybrid machine tool, which would be discussed in Section 6. In kinematic and dynamic modeling, the base coordinate system $O-XY$ shown in Fig. 2 is identical with the real machine coordinate system of the hybrid machine tool such that the kinematic and dynamic models can be applied directly into the control system. A moving coordinate system $O_N-X_NY_N$ is fixed on the tip point of cutter with the Y_N-axis along the vector from points A_2 to B_2. Let the position vector of the tip point of the cutter be $\boldsymbol{r}_{O_N}=[x \quad y]^T$ in the base coordinate system. The position vectors of points A_i and B_i ($i=1,2$) can be expressed as

$$\boldsymbol{r}_{Ai}=[x_{Ai} \quad y_{Ai}]^T=\boldsymbol{r}_{O_N}+\boldsymbol{R}\boldsymbol{r}_{Ai}^N, \quad i=1,2 \tag{2}$$

$$\boldsymbol{r}_{Bi}=[x_{Bi} \quad y_{Bi}]^T=\boldsymbol{r}_{O_N}+\boldsymbol{R}\boldsymbol{r}_{Bi}^N, \quad i=1,2 \tag{3}$$

where $\boldsymbol{R}$ is the rotation matrix from coordinate system $O_N-X_NY_N$ to $O-XY$ and $\boldsymbol{R}=\begin{bmatrix}\cos\alpha & -\sin\alpha\\ \sin\alpha & \cos\alpha\end{bmatrix}$; α is the rotation angle of the moving platform; $\boldsymbol{r}_{Ai}{}^N$ and $\boldsymbol{r}_{Bi}{}^N$ are the position vectors of points A_i and B_i in $O_N-X_NY_N$, $\boldsymbol{r}_{Ai}^N=[0 \quad d_0]^T$ and $\boldsymbol{r}_{Bi}^N=[0 \quad d_0+l_5]^T$; l_5 is the length of the moving platform; and d_0 is the length of the cutter.

According to Fig. 2, the following equations can be obtained

$$\sin\phi_i=\frac{x_{Bi}-x_{Ei}}{l_i}, \quad \cos\phi_i=\frac{y_{Ei}-y_{Bi}}{l_i}, \quad i=1,2 \tag{4}$$

$$\sin\beta_i=\frac{x_{Ai}-x_{Di}}{l}, \quad \cos\beta_i=\frac{y_{Di}-y_{Ai}}{l}, \quad i=1,2 \tag{5}$$

where ϕ_i is the angle between link E_iB_i and the vertical axis parallel to the Y-axis, $0\leqslant\phi_1\leqslant\pi$, $-\pi\leqslant\phi_2\leqslant 0$; β_i is the angle between link A_iD_i and the vertical axis parallel to the Y-axis, $0\leqslant\beta_1\leqslant\pi$, $-\pi\leqslant\beta_2\leqslant 0$; d is the distance between two columns, y_{Bi} is the Y coordinate of point B_i; l_i is the length of the ith extendible link; l is the length of the constant length link; and x_{Ei}, x_{Di} and x_{Bi} are the X coordinates of points E_i, D_i and B_i in $O-XY$.

Based on Eqs. (4) and (5), the inverse kinematic solutions of the mechanism can be written as

$$q_1=y+\cos\alpha\cdot d_0\pm\sqrt{l^2-(x-\sin\alpha\cdot d_0+d/2)^2} \tag{6a}$$

$$q_2=y+\cos\alpha\cdot d_0\pm\sqrt{l^2-(x-\sin\alpha\cdot d_0-d/2)^2} \tag{6b}$$

$$l_1=\sqrt{(x_{B1}+d/2)^2+(y_{B1}-q_1-l_6)^2} \tag{6c}$$

$$l_2=\sqrt{(x_{B1}-d/2)^2+(y_{B1}-q_2-l_6)^2} \tag{6d}$$

where l_6 is the distance between joint points E_i and D_i, $q_i=y_{Di}$, $x_{B1}=x-\sin\alpha\cdot d_0-l_5\sin\alpha$, and $y_{B1}=y+\cos\alpha\cdot d_0+l_5\cos\alpha$. It can be concluded that when one of links A_1D_1 and A_2D_2 is parallel to the X-axis and/or link A_1D_1 is parallel to link A_2D_2, the singularity occurs. To avoid the singularity, it is obvious that $0<|\beta_i|,|\phi_i|<\frac{\pi}{2}$. Thus, the "±" of Eq. (6) should be only '+'.

2.3. Jacobian matrix

The velocity of point A_i can be expressed as

$$\boldsymbol{v}_{Ai}=\boldsymbol{v}+\boldsymbol{\omega}\times\boldsymbol{R}\boldsymbol{r}_{Ai}^N=\boldsymbol{v}+\dot{\alpha}\boldsymbol{E}\boldsymbol{R}\boldsymbol{r}_{Ai}^N, \quad i=1,2 \tag{7}$$

where $\boldsymbol{v}$ is the velocity of the tip point of the cutter, $\boldsymbol{\omega}$ is the angular velocity of the moving platform, and $\boldsymbol{E}=\begin{bmatrix}0 & -1\\ 1 & 0\end{bmatrix}$.

Similarly, the velocity of point B_i can be obtained as

$$\boldsymbol{v}_{Bi} = \boldsymbol{v} + \dot{\alpha}\boldsymbol{E}\boldsymbol{R}\boldsymbol{r}_{Bi}^{\mathrm{N}}, \quad i = 1, 2 \tag{8}$$

Taking the time derivative of Eqs. (4) and (5) leads to

$$\dot{\beta}_i = \dot{x}_{Ai}/(l\cos\beta_i) \tag{9}$$

$$\dot{q}_i = \dot{y}_{Di} = \dot{y}_{Ai} - l\sin\beta_i \cdot \dot{\beta}_i \tag{10}$$

$$\dot{l}_i = \dot{x}_{Bi}\sin\phi_i + (\dot{q}_i - \dot{y}_{Bi})\cos\phi_i \tag{11}$$

$$\dot{\phi}_i = [\dot{x}_{Bi}\cos\phi_i - (\dot{q}_i - \dot{y}_{Bi})\sin\phi_i]/l_i \tag{12}$$

Eq. (10) can be rewritten as

$$\dot{q}_i = -\frac{\sin\beta_i}{\cos\beta_i}\dot{x} + \dot{y} - \left(\sin\alpha + \frac{\sin\beta_i}{\cos\beta_i}\cos\alpha\right)d_o \cdot \dot{\alpha} = \boldsymbol{J}_i\dot{\boldsymbol{p}} \tag{13}$$

where

$$\boldsymbol{J}_i = \left[-\tfrac{\sin\beta_i}{\cos\beta_i} \quad 1 \quad -\left(\sin\alpha + \tfrac{\sin\beta_i}{\cos\beta_i}\cos\alpha\right)d_o\right], \quad \dot{\boldsymbol{p}} = [\dot{x} \quad \dot{y} \quad \dot{\alpha}]^{\mathrm{T}}$$

Eq. (11) can be rewritten as

$$\dot{q}_{i+2} = \dot{l}_i = \boldsymbol{J}_{i+2}\dot{\boldsymbol{p}} = [\sin\phi_i \quad -\cos\phi_i]\left([\boldsymbol{e}_1 \quad \boldsymbol{e}_2]^{\mathrm{T}} + \boldsymbol{E}\boldsymbol{R}\boldsymbol{r}_{Bi}^{\mathrm{N}}\boldsymbol{e}_3^{\mathrm{T}}\right)\dot{\boldsymbol{p}} + \boldsymbol{J}_i\cos\phi_i\dot{\boldsymbol{p}} \tag{14}$$

where

$$\boldsymbol{J}_{i+2} = [\sin\phi_i \quad -\cos\phi_i]\left([\boldsymbol{e}_1 \quad \boldsymbol{e}_2]^{\mathrm{T}} + \boldsymbol{E}\boldsymbol{R}\boldsymbol{r}_{Bi}^{\mathrm{N}}\boldsymbol{e}_3^{\mathrm{T}}\right) + \boldsymbol{J}_i\cos\phi_i\boldsymbol{e}_1 = [1 \quad 0 \quad 0]^{\mathrm{T}}, \quad \boldsymbol{e}_2 = [0 \quad 1 \quad 0]^{\mathrm{T}}, \quad \boldsymbol{e}_3 = [0 \quad 0 \quad 1]^{\mathrm{T}}$$

The velocity equation of the redundant parallel manipulator can be written in the form

$$\dot{\boldsymbol{q}} = \boldsymbol{J}\dot{\boldsymbol{p}} \tag{15}$$

where $\dot{\boldsymbol{q}} = \begin{bmatrix}\dot{q}_1 & \dot{q}_2 & \dot{l}_1 & \dot{l}_2\end{bmatrix}^{\mathrm{T}}$, and $\boldsymbol{J}$ is the Jacobian matrix.

Thus, the Jacobian matrix of the redundantly actuated parallel manipulator studied here, which is a 4×3 matrix, can be expressed as

$$\boldsymbol{J} = [\boldsymbol{J}_1^{\mathrm{T}} \quad \boldsymbol{J}_2^{\mathrm{T}} \quad \boldsymbol{J}_3^{\mathrm{T}} \quad \boldsymbol{J}_4^{\mathrm{T}}]^{\mathrm{T}}. \tag{16}$$

3. Dynamic modeling based on the virtual work principle

3.1. Partial velocity and partial angular velocity matrix

In order to obtain a more compact form of the dynamic model for real-time implementation in the control system, the virtual work principle is employed to derive the dynamic model. Thus, the partial velocity and partial angular velocity matrices, which are used in dynamic modeling, should be first determined. To find the partial velocity matrix, a pivotal point should be selected to have the simplest form of velocity so that the determination of partial velocity matrix can be most efficient. For example, in this paper, the point E_i is regarded as the pivotal point of the slider and the upper part of the extendible link, points B_i, D_i and A_1 are the pivotal points of the lower part of the extendible link, the constant length link and the moving platform in modeling, respectively. The partial velocity matrix of each pivotal point and partial angular velocity matrix of each moving part are computed, respectively.

Since the slider has only translational capability, the partial angular velocity matrix is given by

$$\boldsymbol{G}_{i1} = 0 \tag{17}$$

According to Eq. (10), the partial velocity matrix of point E_i can be expressed as

$$\boldsymbol{H}_{i1} = [0 \quad 1]^{\mathrm{T}}\boldsymbol{J}_i \tag{18}$$

Based on Eqs. (10) and (12), the partial angular velocity matrix of the constant length link and partial velocity matrix of point D_i can be written as

$$\boldsymbol{G}_{i2} = \left[\tfrac{1}{\cos\beta_i \cdot l} \quad 0\right]\left([\boldsymbol{e}_1 \quad \boldsymbol{e}_2]^{\mathrm{T}} + \boldsymbol{E}\boldsymbol{R}\boldsymbol{r}_{Ai}^{\mathrm{N}}\boldsymbol{e}_3^{\mathrm{T}}\right) \tag{19}$$

$$\boldsymbol{H}_{i2} = \boldsymbol{H}_{i1} \tag{20}$$

Similarly, the partial velocity matrix of point E_i and partial angular velocity matrix of the upper part of the extendible link are given, respectively, by

$$\boldsymbol{H}_{i3} = [\,0 \quad 1\,]^{\mathrm{T}}\boldsymbol{J}_i \tag{21}$$

$$\boldsymbol{G}_{i3} = \left[\begin{array}{cc}\frac{\cos\phi_i}{l_i} & \frac{\sin\phi_i}{l_i}\end{array}\right]\left([\,\boldsymbol{e}_1 \quad \boldsymbol{e}_2\,]^{\mathrm{T}} + \boldsymbol{E}\boldsymbol{R}\boldsymbol{r}^{\mathrm{N}}_{Bi}\boldsymbol{e}_3^{\mathrm{T}}\right) - \frac{\sin\phi_i}{l_i}\boldsymbol{J}_i \tag{22}$$

Accordingly, the partial angular velocity matrix of the lower part of link E_iB_i and partial velocity matrix of point B_i can be obtained as

$$\boldsymbol{G}_{i4} = \boldsymbol{G}_{i3} \tag{23}$$

$$\boldsymbol{H}_{i4} = [\,\boldsymbol{e}_1 \quad \boldsymbol{e}_2\,]^{\mathrm{T}} + \boldsymbol{E}\boldsymbol{R}\boldsymbol{r}^{\mathrm{N}}_{Bi}\boldsymbol{e}_3^{\mathrm{T}} \tag{24}$$

Since the counterweight is connected to the slider, the velocity of the counterweight is the negative of that of the slider. Then, based on Eq. (10), the partial angular velocity matrix and partial velocity matrix of the mass center of the counterweight can be expressed as

$$\boldsymbol{G}_{i5} = 0, \quad \boldsymbol{H}_{i5} = [\,0 \quad -1\,]^{\mathrm{T}}\boldsymbol{J}_i \tag{25}$$

The partial angular velocity matrix of the moving platform and partial velocity matrix of point O_{N} can be expressed as

$$\boldsymbol{G}_{\mathrm{N}} = \boldsymbol{e}_3^{\mathrm{T}} \tag{26}$$

and

$$\boldsymbol{H}_{\mathrm{N}} = [\,\boldsymbol{e}_1 \quad \boldsymbol{e}_2\,]^{\mathrm{T}} \tag{27}$$

3.2. Acceleration analysis

Taking the time derivative of Eqs. (7) and (8) leads to

$$\boldsymbol{a}_{Ai} = [\,\ddot{x} \quad \ddot{y}\,]^{\mathrm{T}} + \ddot{\alpha}\boldsymbol{E}\boldsymbol{R}\boldsymbol{r}^{\mathrm{N}}_{Ai} - \dot{\alpha}^2\boldsymbol{R}\boldsymbol{r}^{\mathrm{N}}_{Ai} \tag{28}$$

$$\boldsymbol{a}_{Bi} = [\,\ddot{x} \quad \ddot{y}\,]^{\mathrm{T}} + \ddot{\alpha}\boldsymbol{E}\boldsymbol{R}\boldsymbol{r}^{\mathrm{N}}_{Bi} - \dot{\alpha}^2\boldsymbol{R}\boldsymbol{r}^{\mathrm{N}}_{Bi} \tag{29}$$

where $\boldsymbol{a}_{\mathrm{A}i}$ and $\boldsymbol{a}_{Bi}$ are the acceleration of points A_i and B_i, respectively.

Similarly, taking the time derivative of Eqs. (9)–(12), the angular accelerations $\ddot{\beta}_i$ and $\ddot{\phi}_i$, and the accelerations $\ddot{q}_i$ and $\ddot{l}_i$ can be determined. Thus, the accelerations of point E_i and D_i are given by

$$\boldsymbol{a}_{Ei} = \boldsymbol{a}_{Di} = [\,0 \quad 1\,]^{\mathrm{T}}\ddot{q}_i \tag{30}$$

where $\boldsymbol{a}_{\mathrm{E}i}$ is the acceleration of point E_i, and $\boldsymbol{a}_{\mathrm{D}i}$ is the acceleration of point D_i.

3.3. Inertial forces and moments of moving parts

Utilizing the Newton–Euler equation, the inertial force and moment of each moving part about the pivotal point can be determined. Here, we suppose that m_{i1}, m_{i2}, m_{i3}, m_{i4} and m_{i5} are the masses of the slider, constant length link, the upper part of the extendible link, the lower part of the extendible link and the counterweight, respectively, m_{N} is the mass of the moving platform, $\boldsymbol{g}$ is the gravitational acceleration vector, and $\boldsymbol{g} = [\,0 \quad -9.8\,]^{\mathrm{T}}$.

The inertial force and moment of the slider about point E_i can be expressed as

$$\boldsymbol{F}_{i1} = -m_{i1}(\boldsymbol{a}_{Ei} - \boldsymbol{g}), \quad M_{i1} = 0 \tag{31}$$

The inertial force and moment of the constant length link about point D_i can be expressed as

$$\boldsymbol{F}_{i2} = -m_{i2}\left(\boldsymbol{a}_{Di} + s_{i2}\ddot{\beta}_i\boldsymbol{E}\begin{bmatrix}\sin\beta_i\\ -\cos\beta_i\end{bmatrix} - s_{i2}\dot{\beta}_i^2\begin{bmatrix}\sin\beta_i\\ -\cos\beta_i\end{bmatrix} - \boldsymbol{g}\right) \tag{32}$$

$$M_{i2} = -\ddot{\beta}_i I_{i2} + m_{i2}s_{i2}[\,\sin\beta_i \quad -\cos\beta_i\,]\boldsymbol{E}(\boldsymbol{a}_{Di} - \boldsymbol{g}) \tag{33}$$

where s_{i2} is the distance between the mass center of the constant length link and point D_i, and I_{i2} is the moment of inertia of link A_iD_i about point D_i.

The inertial force and moment of the upper part of the extendible link about point E_i can be written as

$$\boldsymbol{F}_{i3} = -m_{i3}\left(\boldsymbol{a}_{Ei} + s_{i3}\ddot{\phi}_i\boldsymbol{E}\begin{bmatrix}\sin\phi_i\\ -\cos\phi_i\end{bmatrix} - s_{i3}\dot{\phi}_i^2\begin{bmatrix}\sin\phi_i\\ -\cos\phi_i\end{bmatrix} - \boldsymbol{g}\right) \tag{34}$$

$$M_{i3} = -\ddot{\phi}_i I_{i3} + m_{i3}s_{i3}[\,\sin\phi_i \quad -\cos\phi_i\,]\boldsymbol{E}(\boldsymbol{a}_{Ei} - \boldsymbol{g}) \tag{35}$$

where s_{i3} is the distance between the mass center of the upper part of link E_iB_i and point E_i, and I_{i3} is the moment of inertia of the upper part of link E_iB_i about point E_i.

The inertial force and moment of the lower part of link E_iB_i about point B_i can be written as

$$\boldsymbol{F}_{i4} = -m_{i4}\left(\boldsymbol{a}_{Bi} - s_{i4}\ddot{\phi}_i\boldsymbol{E}\begin{bmatrix}\sin\phi_i\\-\cos\phi_i\end{bmatrix} + s_{i4}\dot{\phi}_i^2\begin{bmatrix}\sin\phi_i\\-\cos\phi_i\end{bmatrix} - \boldsymbol{g}\right) \tag{36}$$

$$M_{i4} = -\ddot{\phi}_i I_{i4} - m_{i4}s_{i4}[\sin\phi_i \quad -\cos\phi_i]\boldsymbol{E}(\boldsymbol{a}_{Bi} - \boldsymbol{g}) \tag{37}$$

where s_{i4} is the distance between the mass center of the lower part of extendible link E_iB_i and point B_i, I_{i4} is the moment of inertia of the lower part of the extendible link about point B_i.

The inertial force and moment of the counterweight about its mass center can be written as

$$\boldsymbol{F}_{i5} = -m_{i5}(\boldsymbol{a}_{Pi} - \boldsymbol{g}), \quad M_{i5} = 0 \tag{38}$$

where $\boldsymbol{a}_{Pi}$ is the acceleration of the counterweight.

The inertial force and moment of the moving platform about the point O_N can be expressed as

$$\boldsymbol{F}_N = -m_N\left(\begin{bmatrix}\ddot{x}\\\ddot{y}\end{bmatrix} + \ddot{\alpha}\boldsymbol{E}\boldsymbol{R}\boldsymbol{r}_N - \dot{\alpha}^2\boldsymbol{R}\boldsymbol{r}_N - \boldsymbol{g}\right) \tag{39}$$

$$M_N = -\ddot{\alpha}I_N - m_N([\ddot{x} \quad \ddot{y}] - \boldsymbol{g}^T)\boldsymbol{E}\boldsymbol{R}\boldsymbol{r}_N \tag{40}$$

where $\boldsymbol{r}_N$ is the position vector from the origin of $O_N - X_NY_N$ to the mass center of the platform with respect to $O_N - X_NY_N$, and I_N is the moment of inertia of the moving platform with respect to its mass center.

3.4. Dynamic model and driving force optimization

Based on the virtual work principle, the dynamic formulation of the redundantly actuated parallel manipulator can be expressed as

$$\boldsymbol{J}^T\boldsymbol{\tau} + \sum_{i=1}^{2}\sum_{j=1}^{5}\begin{bmatrix}\boldsymbol{H}_{ij}^T & \boldsymbol{G}_{ij}^T\end{bmatrix}\begin{bmatrix}\boldsymbol{F}_{ij}\\M_{ij}\end{bmatrix} + \begin{bmatrix}\boldsymbol{H}_N^T & \boldsymbol{G}_N^T\end{bmatrix}\begin{bmatrix}\boldsymbol{F}_{ij}\\M_{ij}\end{bmatrix} = 0 \tag{41}$$

where $\boldsymbol{\tau} = [F_1 \quad F_2 \quad F_3 \quad F_4]^T$, F_1, F_2, F_3, and F_4 are the driving forces that act on sliders E_1D_1 and E_2D_2, extendible links E_1B_1, and E_2B_2, respectively.

Since the parallel manipulator has one redundant actuator and $\boldsymbol{J}^T$ is non-square, the driving force $\boldsymbol{\tau}$ in Eq. (41) has infinite solutions. To obtain a unique solution, an optimization technique has to be applied. For different demands, there are different optimizing objectives such as minimizing the two-norm of $\boldsymbol{\tau}$ and minimizing the energy consumed. In this paper, the optimizing objective is to minimize the two-norm of $\boldsymbol{\tau}$. Let $\boldsymbol{\Omega} = -\sum_{i=1}^{2}\sum_{j=1}^{5}\begin{bmatrix}\boldsymbol{H}_{ij}^T & \boldsymbol{G}_{ij}^T\end{bmatrix}\begin{bmatrix}\boldsymbol{F}_{ij}\\M_{ij}\end{bmatrix} - \begin{bmatrix}\boldsymbol{H}_N^T & \boldsymbol{G}_N^T\end{bmatrix}\begin{bmatrix}\boldsymbol{F}_{ij}\\M_{ij}\end{bmatrix}$, the solution of Eq. (41) to minimize the two-norm of $\boldsymbol{\tau}$ by the least-square method is determined by

$$\boldsymbol{\tau}_{min} = \boldsymbol{J}\left(\boldsymbol{J}^T\boldsymbol{J}\right)^{-1}\boldsymbol{\Omega} \tag{42}$$

It can be proved as follows. Let $\boldsymbol{\tau}^* = \boldsymbol{J}(\boldsymbol{J}_T\boldsymbol{J})^{-1}\boldsymbol{\Omega}$ and $\boldsymbol{\tau}_x$ be the other solution of Eq. (41). Further, let $\boldsymbol{y} = \boldsymbol{\tau}_x - \boldsymbol{\tau}^*$, the following formula can be obtained:

$$\|\boldsymbol{\tau}_x\|^2 = \|\boldsymbol{\tau}^* + \boldsymbol{y}\| = \|\boldsymbol{\tau}^*\|^2 + 2\left(\boldsymbol{J}\left(\boldsymbol{J}^T\boldsymbol{J}\right)^{-1}\boldsymbol{\Omega}, \boldsymbol{y}\right) + \|\boldsymbol{y}\|^2 \geqslant \|\boldsymbol{\tau}^*\|^2 + \|\boldsymbol{y}\|^2 > \|\boldsymbol{\tau}^*\|^2 \tag{43}$$

Thus, it has $\boldsymbol{\tau}^* = \boldsymbol{\tau}_{min}$.

4. Control scheme

In theory, a redundantly actuated parallel manipulator in a low speed can be controlled only by the position mode. However, in practical motion, it is very difficult to obtain the real values of many parameters though some identification technologies have been developed. In addition, there are errors in the position control loop. Thus, if the redundant chain is also controlled by position mode, the interference between redundant link and other links will be caused such that great internal forces are introduced and the deflections of the links are expanded. As a result, the absolute positioning and orienting errors are increased and the mechanism is even collapsed. It can be seen that the use of mere position control is no longer possible.

When only the redundant actuator moves and other actuators are locked, the moving platform can not move unless the parallel manipulator reaches its singular configuration. Thus, it can be argued that actuation redundancies are force redundancies in some sense. A simple and effective control strategy is that the redundant chain is controlled by the force mode [29] and other chains the position mode [30]. When the redundant manipulator reaches the configuration that link E_2B_2 and the moving platform A_2B_2 are collinear, the redundant chain can drive the parallel manipulator to pass the configuration. Moreover, there are clearance, deflection and vibration in the manipulator. The internal force of redundant chain can be effectively utilized to reduce them.

As a result, the position and orientation accuracy of the redundant parallel manipulator is guaranteed by those non-redundant chains. The redundant chain devotes itself to improve the manipulator performances such as stiffness, dexterity

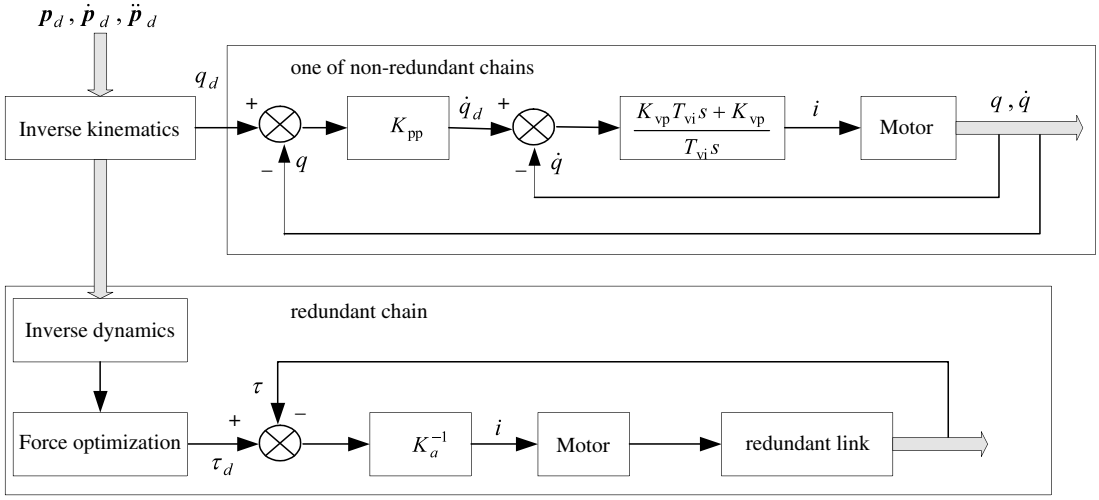

Fig. 3. Control scheme of the redundantly actuated parallel manipulator.

Table 1
Control system parameters of the non-redundant chain

Parameter	Definition	Unit
K_{ip}	Proportional coefficient of current loop	V/A
K_{pp}	Proportional coefficient of position loop	V/mm
T_{ii}	Integral coefficient of current loop	s
K_{vp}	Proportional coefficient of velocity loop	A s/rad
T_{vi}	Integral coefficient of velocity loop	s
J	inertia of motor rotor and screw	Kg m^2
L	Winding inductance	H
R	Winding resistance	Ω
K_t	Magnetic torque coefficient	N m/A
K_e	Back electromotive force coefficient of motor	V s/rad

and dynamic characteristics. The servo drivers of the control system of non-redundant chain provide proportional control for position loop, proportional–integral (PI) control for velocity loop, and PI control for current loop. The control scheme of the redundant parallel manipulator is shown in Fig. 3. $\boldsymbol{p}_d$, $\dot{\boldsymbol{p}}_d$ and $\ddot{\boldsymbol{p}}_d$ are the desired position, velocity and acceleration of the moving platform, τ_d and τ are the desired and actual force, and K_a is the exchanging coefficient from force to current of the motor.

The open-loop transfer function of the control system of the non-redundant chain can be expressed as

$$G_1(s) = \frac{q(s)}{q_d(s)} = K_{pp}\frac{K_t K_{ip} K_{vp}\left[T_{ii}T_{vi}s^2 + (T_{ii} + T_{vi})s + 1\right]}{JLT_{ii}T_{vi}s^5 + JT_{ii}T_{vi}(R + K_{ip})s^4 + C_{s3}s^3 + K_t K_{ip} K_{vp}(T_{ii} + T_{vi})s^2 + K_t K_{ip} K_{vp} s} \tag{44}$$

where $C_{s3} = JK_{ip}T_{vi} + K_e K_t T_{ii} T_{vi} + K_t K_{ip} K_{vp}\, T_{ii} T_{vi}$, q and q_d are the actual and desired rotation angle of the servo-motor rotor, and other parameters are given in Table 1.

5. Application of the control strategy

5.1. Position and force switching control

From the above analysis, it can be seen that the control strategy that link E_1B_1 is controlled by the force mode and link E_2B_2 the position mode can improve the manipulator performance. However, this control strategy cannot be implemented in the whole workspace. The reasons are given as follows. (1) The configuration that link E_2B_2 and the moving platform A_2B_2 are collinear is the singular configuration of the non-redundant manipulator without link E_1B_1. Although the singular configuration cannot occur in the redundant manipulator, it is very difficult to assure the position accuracy of link E_2B_2 with position mode when the redundant manipulator is near the configuration that link E_2B_2 and the moving platform A_2B_2 are collinear. In order to pass the configuration, a force, which is provided by link E_1B_1, should act on the joint point $B_1(B_2)$. But, the position accuracy of link E_1B_1 cannot be assured by the force mode such that the motion accuracy of the manipulator in or near this configuration is worse. (2) In theory, the servo-driver of link E_2B_2 can receive accurate position command and the axial velocity of link E_2B_2 is zero when the manipulator reaches the configuration that link E_2B_2 and the moving platform A_2B_2 are

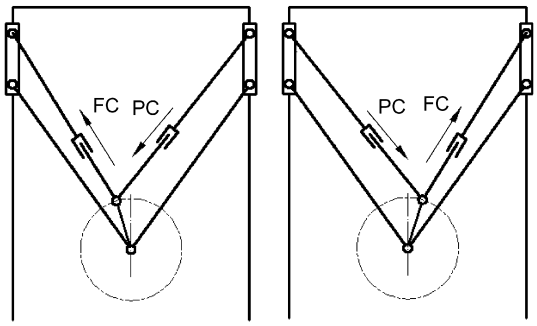

Fig. 4. Sketch of control mode for extendible links (a) $\alpha \geqslant 0^\circ$ and (b) $\alpha < 0^\circ$.

collinear. However, in the control system, the motion of the manipulator is point-to-point, and it is very difficult to ensure that there is no increment in the axial direction of link E_2B_2. Thus, a great internal force will be produced between link E_2B_2 and the moving platform A_2B_2.

In order to ensure the position and orientation accuracy of the redundant manipulator and pass the configuration that link E_1B_1 or E_2B_2 and the moving platform A_2B_2 are collinear, a position and force switching control strategy is proposed for the redundantly actuated parallel manipulator. In this control strategy, the two extendible links are controlled by position and force modes, respectively. When one of the extendible links reaches or approaches the configuration that it and the moving platform A_2B_2 are collinear, the extendible link is controlled by the force mode and the other extendible link by the position mode, as shown in Fig. 4. In Fig. 4, FC and PC denote the force control mode and the position control mode, respectively. At one time, one of the extendible links is the force mode and the other link must be position mode.

5.2. Critical angle for switching control modes

From Fig. 4, it can be seen that the control mode of each extendible link should be changed in the whole workspace. This involves the critical value of α where the control modes of the extendible links are switched. Since the redundant manipulator is symmetrical, it would be ideal to select $\alpha = 0$ as the critical angle. However, the switching of control modes would be much more frequent, since the manipulator maybe has a reciprocating motion in $\alpha = 0$. Furthermore, the switching of control mode brings different reference benchmarks for position mode and results in some errors from different benchmarks.

Thus, the critical angle for switching the control modes should be planned by real demands to reduce the switching frequency of the control mode. At the meantime, the configuration in the critical angle should be far from the configuration that link E_1B_1 or E_2B_2 and the moving platform A_2B_2 are collinear. In addition, the critical angles should be symmetrical about the Y-axis due to the symmetry of the parallel manipulator. Based on these considerations, in this paper, three critical angles are specified. Namely, $\alpha = 0$, $\alpha = 5^0$and $\alpha = -5^0$. It should be pointed out that the control modes are not always switched when the moving platform rotates to one of the critical angles.

In the numerical control system of the redundantly actuated parallel manipulator, there are four main modular. Namely, post-processing, trajectory planning, interpolation and real-time module. In trajectory planning phase, an input trajectory may be separated into many trajectory segments. It is necessary to determine whether the control modes of the extendible links in each trajectory segment should be switched. The switching of control modes is related to the control mode of the last trajectory segment, the start value α_s and the end value α_e of the rotation angle α in the current trajectory segment. The switching rule is given as follows:

(1) The control mode keeps unchanged when the rotation angle α ranges from -5^0 to 5^0. In the range, the orientation has little effect on the performance of the redundant parallel manipulator.
(2) When $\alpha > 5^0$, link E_1B_1 is controlled by force mode and link E_2B_2 is position mode. On the contrary, link E_1B_1 is position mode and link E_2B_2 is force mode when $\alpha < -5^0$.
(3) When link E_1B_1 is controlled by the force mode, it is assumed that $m = 1$. The position mode corresponds to $m = -1$.

Based on above rules, the condition for switching the control modes is determined, as shown in Table 2.

5.3. Position compensation

When the extendible link is under force mode, the lengthened or shortened deformation would be produced such that there are difference between the theoretical length of extendible link and actual length. In the trajectory plan and interpolation module of the control system, the theoretical length in the current interpolation period is regarded as the benchmark

Table 2
Condition for switching control modes

Motion condition	switching of control modes	Critical angle
$\|\alpha_s\| > 5$, $\|\alpha_e\| > 5$, $\alpha_s\alpha_e < 0$	Yes	0
$\|\alpha_s\| \leqslant 5$, $\|\alpha_e\| > 5$, $\alpha_e m < 0$	Yes	$-5m$
Other	No	/

to plan the length of extendible link in the next period. In one period, it is possible that the extendible link lengthens/shortens a long distance to the theoretical length when the control mode ranges from force mode to position mode. If the moving distance of the extendible link is larger than the limit value in one period, the servo error would be given. Thus, the difference between the theoretical length and actual length of the extendible link should be compensated when the control mode of the extendible link changes from the force mode to position mode. It is aimed to adjust the extendible distance of the extendible link in a few periods such that the theoretical length and actual length are identical.

Let the actual length and theoretical length of the extendible link with force mode be l_0 and l_T, the difference between l_0 and l_T can be expressed as

$$e_l = l_T - l_0 \tag{45}$$

The lengthened or shortened length of the link in one interpolation period can be written as

$$l_\Delta = vT \tag{46}$$

where l_Δ is the lengthened or shortened length, v is the moving velocity, and T is the interpolation period.

In one period, the maximum lengthened or shortened length can be written as

$$l_{\max} = v_{\max} T \tag{47}$$

where $v_{\max}$ is the maximum moving velocity which can be given in the servo-driver.

In one period, the difference between the maximum extendible length and actual extendible length of the extendible link can be expressed as

$$e_\Delta = l_{max} - l_\Delta \tag{48}$$

If $l_0 < l_T$ and the link is needed to lengthen, the link should move with the maximum velocity $v_{\max}$ in n_1 periods after the control modes are switched. n_1 can be expressed as

$$n_1 = \frac{|e_l|}{e_\Delta} \tag{49}$$

The moving distance in the $(n_1 + 1)$th period can be expressed as

$$s_1 = vT + |e_l| - n_1(v_{\max} T - vT) \tag{50}$$

On the contrary, if $l_0 < l_T$ and the link is needed to shorten, the extendible link should not move in n_2 periods after the control modes are switched. n_2 can be expressed as

$$n_2 = \frac{|e_l|}{vT} \tag{51}$$

The moving distance in the $(n_2 + 1)$th period can be expressed as

$$s_2 = |e_l| - n_2 vT \tag{52}$$

If $l_0 > l_T$, the moving rule of the extendible link can be analyzed in the same way.

When $\alpha = 0$, the machine has a symmetrical configuration. It can be thought that the actual length of the extendible link is the same as the theoretical length. Thus, the position compensation is not needed when the control modes are switched at $\alpha = 0$. When $\alpha = \pm 5^0$, the extendible link is lengthened or shortened and the actual length dose not equal the theoretical length. Then, the position compensation is necessary when the control modes are switched at $\alpha = \pm 5^0$.

6. Experiments

As an example to optimize the driving force, the geometrical and inertial parameters of the parallel manipulator are given in Tables 3 and 4, respectively.

The redundantly actuated parallel manipulator is incorporated into a 4-DOF hybrid machine tool, which also includes a feed worktable as shown in Fig. 5. The sensors for sliders E_1D_1 and E_2D_2 are linear grating sensors, and the motor encoders on links E_1B_1 and E_2B_2 are absolute and incremental, respectively. The control strategy proposed in this paper has been applied into the numerical control system. The interpolation period is 2 ms. The force, which is the input of the extendible chain with force mode, should be obtained by the feedback value of the force sensors in practical machining. However, at present, the

Table 3
Geometrical parameters

Parameter	Value
d (m)	1.17
d_0 (m)	0.35
l (m)	1.15
l_5 (m)	0.25
l_6 (m)	0.25

Table 4
inertial parameters

	$i = 1$	$i = 2$
m_N (kg)	150	150
m_{i1} (kg)	120	120
m_{i2} (kg)	220	220
m_{i3} (kg)	60	60
m_{i4} (kg)	20	20
m_{i5} (kg)	495	495
I_{i2} (kg m^2)	105.6	105.6
I_{i3} (kg m^2)	7.2	7.2
I_{i4} (kg m^2)	4.27	4.27

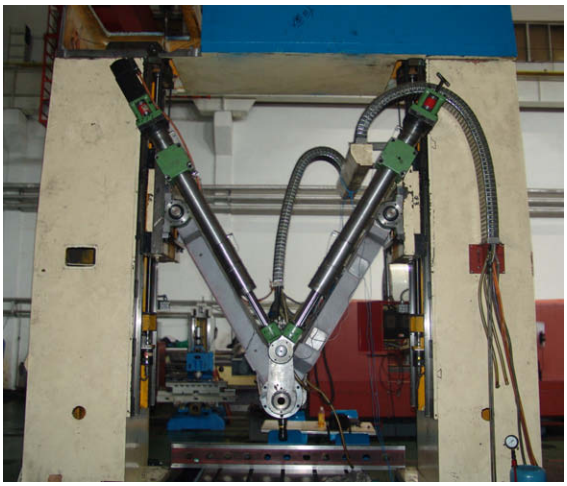

Fig. 5. Photograph of the hybrid machine tool.

force sensors have not been added to the machine tool. Considering that the tests in this paper are done with null-run of the machine tool, the external force and moment can be approximately regarded as zero. Thus, the input force of the extendible chain with force mode can be obtained by the inverse dynamic model. The dynamic model is added into the interpolation module of the numerical control system. In practical application, before the machine tool can be used to machine, it is necessary to perform the homing procedure to return to the machine's zero point [31]. After homing, $\alpha = 0$ and link E_1B_1 is set to be controlled by the force mode and other links are position mode.

In the test, the moving platform moves from the point with the coordinate (-0.15 m, 0.35 m, $-4°$) to another point with the coordinate (0.15 m, 0.35 m, 14°), and the feed speed of the moving platform is 1.8 m/min. The data sampling period is 0.1 s. The driving forces of the redundantly actuated parallel manipulator and its corresponding non-redundant manipulator, which are the commanded forces in the control system, are shown in Figs. 6 and 7, respectively. For the same movement, the driving forces in both redundant and non-redundant cases change smoothly. However, compared with the driving force acting on the extendible link of the non-redundant manipulator, the driving forces acting on the two extendible links of the redundant manipulator have a small range. It can be concluded that the dynamic performance of the redundant parallel manipulator is better than that of the corresponding non-redundant manipulator.

In order to compare the contouring performance of the redundant parallel manipulator with that of its corresponding non-redundant one with the link E_1B_1 disassembled, a linear trajectory and circular trajectories are planned. In the experiments, the redundant parallel manipulator and the non-redundant manipulator move along the linear or circular trajectory,

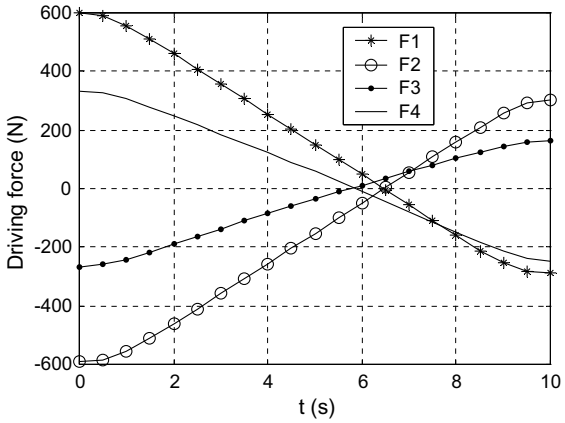

Fig. 6. Driving forces of redundant manipulator.

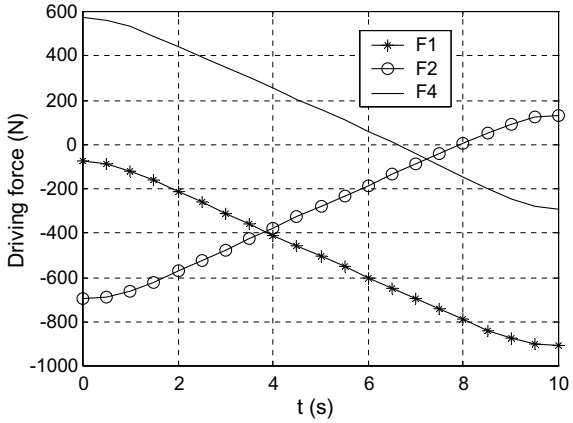

Fig. 7. Driving forces of non-redundant manipulator.

respectively. The contour errors that the manipulator moves along the same trajectory with different velocities are measured. The start point of the linear trajectory is (−0.1 m, 0.35 m, −4°), the end point is (0.15 m, 0.35 m, 14°), and the moving velocities vary from 500 mm/min to 3000 mm/min. The contour errors that the redundant parallel manipulator and the corresponding non-redundant parallel manipulator move along the linear trajectory are shown in Fig. 8. The contour error

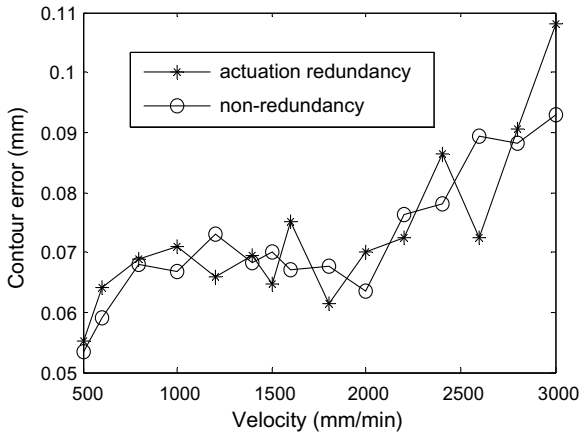

Fig. 8. Linear contouring performance.

increases when the velocity varies from 500 mm/min to 3000 mm/min. The contour error of the redundant parallel manipulator is slightly larger than that of the corresponding non-redundant parallel manipulator.

In the circular trajectory experiment, the radius is 50 mm, and the moving velocity ranges from 400 mm/min to 2200 mm/min. In addition to the conventional circular contour test, a small-circle test is performed on the machine. This test is especially useful in gauging the contouring behavior of the machine when producing small spatial features (such as small-circles, sharp corners, etc.) where the behavior of the system may be dominated by non-linear effects such as friction, axis backlash, etc. For this test, a circle of radius 2 mm is chosen and the speed is varied from 100 mm/min to 1500 mm/min. Figs. 9 and 10 give the contour errors of circular trajectories with radius 2 mm and 50 mm, respectively. The contour error between the desired trajectory and the actual trajectory increases approximately with the increase of the moving velocity.

To study the response of the system to increase in frequency (angular velocity ω) without the confounding effects of simultaneously varying the maximum angular acceleration, the radius r of the circle is varied along with the angular velocity (to keep $\omega^2 r$ constant). The feedrate and radius are varied in the range of 100 mm/min to 1200 mm/min and 0.013888 mm to 2 mm. The contour error that the manipulator moves along the circular trajectories with constant maximum acceleration is shown in Fig. 11. The contour errors that the manipulator in both redundant and non-redundant cases moves along the circular trajectories increase approximately with the increase of the velocity. However, the contour error that the non-redundant parallel manipulator moves along the circular trajectory changes abruptly.

Fig. 12 is the tracking error of chain E_2B_2 in redundant and non-redundant cases when the machine tool moves along the circular trajectory of radius 50 mm and speed 1800 mm/min. In theory, the tracking error of link E_2B_2 should be zero since the rotation angle keeps unchanged. In fact, it can be seen that the tracking errors of link E_2B_2 in both redundant and non-redundant cases vary in approximately sinusoidal manner. It can be concluded that there is clearance in link E_2B_2. Due to the introduction of link E_1B_1, the clearance in link E_2B_2 of the redundant parallel manipulator is smaller than that of the corre-

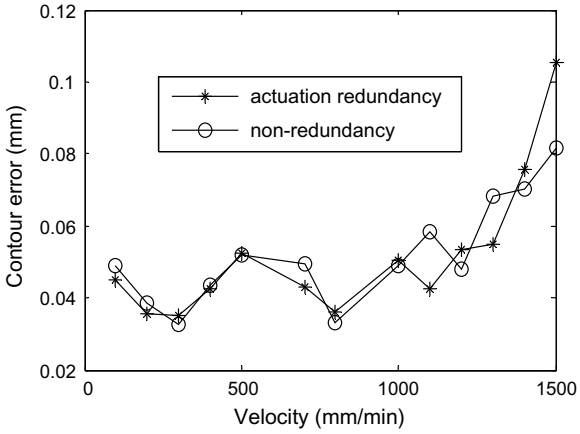

Fig. 9. Circular contouring performance with radius 2 mm.

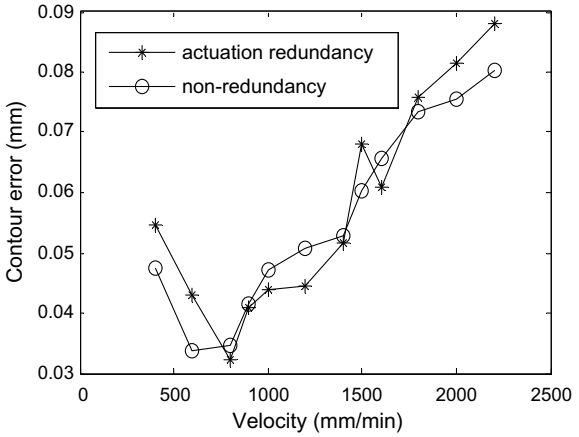

Fig. 10. Circular contouring performance with radius 50 mm.

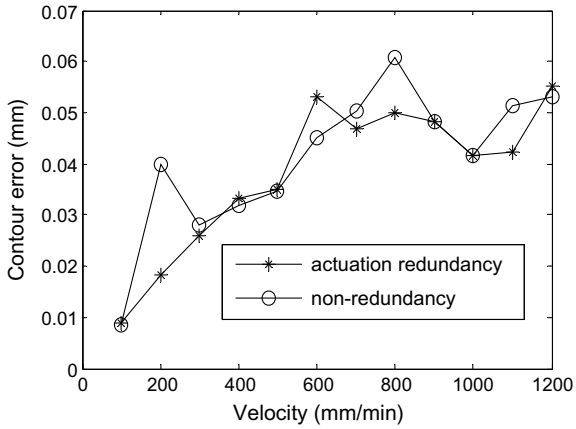

Fig. 11. Small-circle contour errors with constant maximum acceleration.

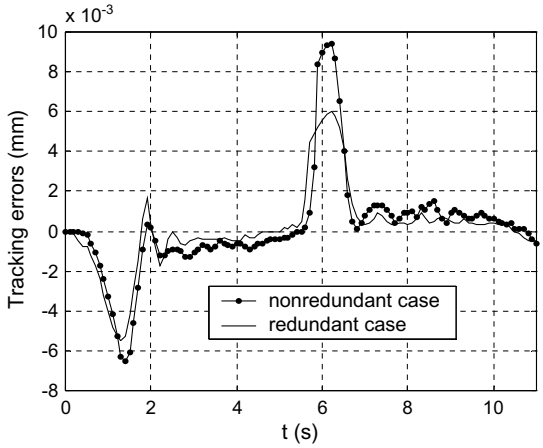

Fig. 12. Tracking errors of link E_2B_2.

sponding non-redundant manipulator. Accordingly, the tracking error of link E_2B_2 of the redundant manipulator is smaller than that of the corresponding non-redundant manipulator.

From above analysis, one may see that the contour error of the redundant manipulator is similar to that of its corresponding non-redundant manipulator. However, the redundant parallel manipulator has larger orientation workspace, better dexterity and higher stiffness, as addressed in the literature [32]. To demonstrate its applicability, a machining test that machining a blade of gas turbine has been done, as shown in Fig. 13. The machined blade meets the demand of a company in China.

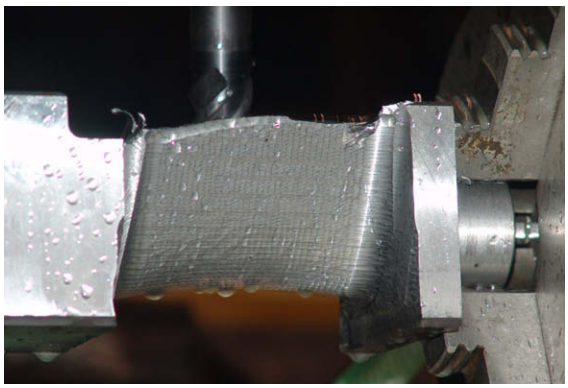

Fig. 13. Machining blade test.

7. Conclusions

This paper has investigated the dynamics and control of a redundantly actuated parallel manipulator. From this investigation, the following conclusions can be drawn:

(1) Utilizing the virtual work principle, the dynamic model of the redundantly actuated parallel manipulator is obtained and the driving force is optimized by least-square method.
(2) A position and force switching control strategy is proposed for the two extendible chains. $\alpha = 0$, $\alpha = 5^0$ and $\alpha = -5^0$ are regarded as the possible critical angles for switching the control modes of the extendible links. The condition for switching the control modes is determined by the control mode of the last trajectory segment, α_s and α_e of the current trajectory.
(3) Due to the introduction of link E_1B_1, the clearance in link E_2B_2 of the redundant parallel manipulator is smaller than that in link E_2B_2 of the corresponding non-redundant parallel manipulator.
(4) With the same trajectory, the contour error of the redundant manipulator is similar to that of the corresponding non-redundant manipulator. By combining the redundantly actuated parallel manipulator with a feed worktable, a hybrid machine tool is created.

Acknowledgements

This work is supported by the National Nature Science Foundation of China (Grant Nos. 50775117 and 50775125), Scientific and Technical Essential Program (Grant No. 2006BAF01B09), and the 973 Program of China (Grant No. 2006CB705400).

The authors gratefully acknowledge the discussion on the paper with Professor Xin-Jun Liu.

References

[1] J. Sefrioui, C.M. Gosselin, On the quadratic nature of the singularity curves of planar three-degree-of-freedom parallel manipulators, Mech. Mach. Theory 30 (4) (1995) 533–551.
[2] C.L. Collins, G.L. Long, Singularity analysis of an in-parallel hand controller for force-reflected teleoperation, IEEE Trans. Rob. Autom. 11 (5) (1995) 661–669.
[3] J. Wu, J.S. Wang, T.M. Li, L.P. Wang, Analysis and application of a 2-DOF planar parallel mechanism, ASME J. Mech. Des. 129 (4) (2007) 434–437.
[4] B. Dasgupta, T.S. Mruthyunjaya, Force redundancy in parallel manipulators: theoretical and practical issues, Mech. Mach. Theory 33 (6) (1998) 727–742.
[5] P. Buttolo, B. Hannaford, Advantages of actuation redundancy for the design of haptic displays, in: Proceedings of ASME International Mechanical Engineering Congress and Exposition, San Francisco, CA, USA, 1995, pp. 623–630.
[6] J. Wang, C.M. Gosselin, Kinematic analysis and design of kinematically redundant parallel mechanisms, ASME J. Mech. Des. 126 (1) (2004) 109–118.
[7] S.B. Nokleby, R. Fisher, R.P. Podhorodeski, F. Firmani, Force capabilities of redundantly actuated parallel manipulators, Mech. Mach. Theory 40 (5) (2005) 578–599.
[8] A. Zibil, F. Firmani, S.B. Nokleby, R.P. Podhorodeski, An explicit method for determining the force-moment capabilities of redundantly actuated planar parallel manipulators, ASMW J. Mech. Des. 129 (10) (2007) 1046–1055.
[9] F. Firmani, R.P. Podhorodeski, Force-unconstrained poses for a redundantly actuated planar parallel manipulator, Mech. Mach. Theory 39 (5) (2004) 459–476.
[10] J.-P. Merlet, Redundant parallel manipulators, Lab. Rob. Autom. 8 (1) (1996) 17–24.
[11] M. Nahon, J. Angeles, Real-time force optimization in parallel kinematic chains under inequality constraints, IEEE Trans. Rob. Autom. 8 (4) (1992) 439–450.
[12] B.-J. Yi, I.H. Suh, S.-R. Oh, Analysis of a 5-bar finger mechanism having redundant actuators with applications to stiffness and frequency modulations, in: Proceedings of the 1997 IEEE International Conference on Robotics and Automation, Albuquerque, NM, USA, 1997, pp.759–765.
[13] B.-J. Yi, S.-R. Oh, I.H. Suh, Five-bar finger mechanism involving redundant actuators: analysis and its applications, IEEE Trans. Rob. Autom. 15 (6) (1999) 1001–1010.
[14] H.W. Kim, J.H. Lee, I.H. Suh, B.-J. Yi, Comparative study and experimental verification of singular-free algorithms for a 6 DOF parallel haptic device, Mechatronics 15 (4) (2005) 403–422.
[15] J. Kim, F.C. Park, S.J. Ryu, J. Kim, J.C. Hwang, C. Park, C.C. Iurascu, Design and analysis of a redundantly actuated parallel mechanism for rapid machining, IEEE Trans. Rob. Autom. 17 (4) (2001) 423–434.
[16] J.S. Wang, J. Wu, L.P. Wang, T.M. Li, Simplified strategy of the dynamic model of a 6-UPS parallel kinematic machine for real-time control, Mech. Mach. Theory 42 (9) (2007) 1119–1140.
[17] C.D. Zhang, S.M. Song, An efficient method for inverse dynamics of manipulators based on the virtual work principle, J. Rob. Syst. 10 (5) (1993) 605–627.
[18] K. Yamane, Y. Nakamura, M. Okada, N. Komine, K. Yoshimoto, Parallel dynamics computation and H infinity acceleration control of parallel manipulators for acceleration display, ASME J. Dyn. Syst., Meas., Control 127 (2) (2005) 185–191.
[19] Z. Zhu, J. Li, Z. Gan, H. Zhang, Kinematic and dynamic modelling for real-time control Tau parallel robot, Mech. Mach. Theory 40 (9) (2005) 1051–1067.
[20] G.F. Liu, Y.L. Wu, et al., Analysis and control of redundant parallel manipulators, in: Proceedings of the 2001 IEEE International Conference on Robotics and Automation, Seoul, South Korea, 2001, pp. 3748–3754.
[21] H. Cheng, Y.K. Yiu, Z.X. Li, Dynamics and control of redundantly actuated parallel manipulators, IEEE/ASME Trans. Mech. 8 (4) (2003) 483–491.
[22] L. Ganovski, P. Fisette, J.C. Samin, Piecewise overactuation of parallel mechanisms following singular trajectories: Modeling, simulation and control, Multibody Syst. Dyn. 12 (4) (2004) 317–343.
[23] T. Ropponen, Actuation redundancy in a closed-chain robot mechanism, Ph.D., dissertation, Helsinki University of Technology, Finland, 1993.
[24] D. Chakarov, Study of the antagonistic stiffness of parallel manipulators with actuation redundancy, Mech. Mach. Theory 39 (6) (2004) 583–601.
[25] A. Muller, Internal preload control of redundantly actuated parallel manipulators – Its application to backlash avoiding control, IEEE Trans. Rob. 21 (4) (2005) 668–677.
[26] S. Koch, W. Schumacher, Control of a fast parallel robot with a redundant chain and gearboxes: experimental results, in: Proceedings of the 2000 IEEE International Conference on Robotics and Automation, San Francisco, CA, USA, 2000, pp. 1924–1929.
[27] H. Shen, X.Z. Wu, G.F. Liu, Z.X. Li, Hybrid position/force adaptive control of redundantly actuated parallel manipulators, Zidonghua Xuebao/Acta Automat. Sin. 29 (4) (2003) 567–572.

[28] B. Kvtoslav, J. Bohm, M. Valasek, State-space generalized predictive control for redundant parallel robots, Mechanics Based Design of Structures and Machines, Special Issue on Virtual Nonlinear Multibody Systems 31(3) (2003) 413–432.
[29] Y.-R. Hu, G. Vukovich, Position and force control of flexible joint robots during constrained motion tasks, Mech. Mach. Theory 36 (7) (2001) 853–871.
[30] Y. Su, D. Sun, L. Ren, J.K. Mills, Integration of saturated PI synchronous control and PD feedback for control of parallel manipulators, IEEE Trans. Rob. 22 (1) (2006) 202–207.
[31] J.S. Wang, J. Wu, L.P. Wang, T.M. Li, Homing strategy for a redundantly actuated parallel kinematic machine, ASME J. Mech. Des. 130 (4) (2008) 0445011–0445015.
[32] J. Wu, J.S. Wang, T. Li, L.P. Wang, Performance analysis and application of a redundantly actuated parallel manipulator for milling, J. Intell. Rob. Syst. 50 (2) (2007) 163–180.